Electronic States of Dislocations in Semiconductors

Kinichi Masuda-Jindo

Department of Materials Science and Engineering, Tokyo Institute of Technology, Nagatsuta 4259, Midoriku, Yokohama 227, Japan

The atomic configurations and electronic states of dislocations in covalent semiconductors are studied using an LCAO (linear combination of atomic orbitals) recursion electronic theory. Partiqular attention will be focused on the determination of band gap states associated with the dislocation line and point like singularities, "solitons", in the dislocation core region. Using the calculated electronic states of the dislocations, we discuss the effects of impurity doping and non-radiative recombination of the injected carriers on the dislocation motion in the semiconductors.

1. INTRODUCTION

It has been well established that the dislocation mobility in semiconductors is affected quite significantly by doping of electrically active impurities [1,2]. The effect of n-doping is quite large for Si and Ge, and it increases the dislocation velocity by reducing the apparent activation energy of dislocation motion. The behavior of p-doping is anomalous, but for high concentrations of acceptors, the velocity also increases (decreases) when compared with intrinsic Si (Ge). On the other hand, dislocation motion in covalent semiconductors (e.g., GaAs, InP, GaP and Si) is strongly enhanced by irradiation by electron beam or laser light [2,3]. The observed excitation enhancement of the dislocation motion can be interpreted in terms of the reduction in activation energy of non-radiative recombination of injected carriers at the dislocation core [5]. In the present study, we focus our attention to the electronic states associated with dislocations in covalent semiconductors. We calculate the atomic configurations and local electronic states of dislocations in Si crystals using the LCAO (linear combination of atomic orbitals) recursion electronic theory [6,7].

Using the calculated electronic states of the dislocations, we also discuss the effects of impurity doping and non-radiative recombination of the injected carriers on the dislocation motion in the semiconductors. We will show that the point like singularities "solitons" exsisting in the reconstructed core are responsible for the deep levels of the dislocation cores. This conclusion is identical to that of the earlier work by Heggie and Jones [8] in the sense that point like irregularities play an important role in the elemental process of the dislocation motion. However, the present calculations are in distinction with the previous ones in the following points: We have found that "solitons" in the reconstructed dislocation core with very small atomic displacements (for details, see Fig.1) can produce the prominent deep levels in the band gap. This is in accordance with the recent theoretical speculation by Maeda and Takeuchi [5] on the dislocation mobility and experimental result on the

dislocation core using the high resolution electron microscopy observations [9].

2. PRINCIPLE OF CALCULATIONS

To calculate the atomic configuration of the dislocation core, we use the LCAO recursion theory and the quenched molecular dynamics method [10,11]. We assume that the total energy of the system can be given by a sum of the band structure energy E_b and the pairwise repulsive energy E_r contributions. The band structure energy E_b can be calculated from the electronic Green's functions of the continued fraction form.

$$G_{ii}(E) = 1/[E - a_1 - b_1/(E - a_2 - \ldots - b_n/(E - a_{n+1} - b_{n+1}/E -], \quad (1)$$

where a_i and b_i are the recursion coefficents and obtained by usual recursion technique.[6] The local density of staes (DOS) $\rho_i(E)$ on atomic site i can then be calculated from the Green's function $G_{ii}(E)$ as

$$\rho_i(E) = -(1/\pi) \lim_{s \to 0} \mathrm{Im}\, G_{ii}(E+is) \quad (2)$$

The two center hopping integrals and pairwise repulsive potentials are taken from Refs. 12 and 13, and used for the atomic configuration calculation of the dislocations. This set of transferable TB parameters reproduces well the equilibrium volumes of close packed structures of Si and is suitable for extensive molecular dynamics simulations [12-14]. In general, the functional forms of the two center integrals and repulsive potentials are introduced so as to have a rapid attenuation between the first- and second-neighbours in the diamond structure. On the other hand, the minimal basis sp^3s^* basis functions proposed by Vogl et al. [15] are used for the electronic structure calculations of the dislocations. This choice of TB parameters are based on the following reasons; The usual nearest-neighbour sp^3 model fails to produce an indirect gap for Si because it omits essential physics; the excited atomic states, such as the s* state of atomic Si, couple with the anti-bonding p-like conduction states near the X and L points of the Brillouin zone, and press these states down in energy. Therefore, the inclusion of an excited s-state, s*, on each atom is essential, giving an sp^3s^* basis and a ten-band theory. This model has been applied to interpret successfully data on point defects, bulk and surface core excitons and semiconductor surface states. The atomic energy levels E_s, E_p and E_{s^*} are shifted rigidly so as to ensure the local charge neutrality condition in the crystal with dislocations

To terminate the recursion coefficients, we use two different termination schemes: (1) For the atomic configuration calculation of the dislocation, we use the simple termination scheme proposed by Beer and Pettifor [16], with the exact recursion coefficients up to the fourth level. We use the more elaborate average termination procedure of Ref.7 for the electronic structure calculation of the dislocations: The recursion coefficients are calculated up to 34th level for the clusters of about 32800 atoms.

Table 1. TB parameters used in the present calculation (eV).

material	E_s	E_p	E_s^*	ssσ	spσ	s*pσ	ppσ	ppπ
C	-4.545	3.840	11.37	-5.681	6.591	3.555	6.795	-1.958
Si	-4.2	1.715	6.69	-2.075	2.481	2.327	2.716	-0.715
Ge	-5.88	1.61	6.39	-1.695	2.366	2.260	2.853	-0.823

The atomic relaxation calculation is preformed by using the quenched molecular dynamics method, i.e., by integrating the Newtonian equation of motion with the central difference algolithm [10,11]. We use the following explicit expressions:

$$r_i(t+\Delta t) = 2r_i(t) - r_i(t-\Delta t) + [F_i(t)/m]\Delta t^2 + 0(\Delta t^4) \ , \quad (3)$$

$$v_i(t) = (1/2)[r_i(t+\Delta t)-r_i(t-\Delta t)/\Delta t] + 0(\Delta t^3) \ , \quad (4)$$

where $r_i(t)$, $v_i(t)$ are the position and velocity of the atom i at time t and $F_i(t)$ is the force acting on the atom i at this time. The minimum energy atomic configuration can be determined by using the quenching procedure, i.e., the velocity of an atom i is cancelled when the product $F_i(t)v_i(t)$ is negative.

3. RESULTS AND DISCUSSIONS

In a diamond cubic crystal, the important dislocations are the 60° , screw and 90° (edge) perfect dislocations [17]. The first one dissociates into a 30° and 90° partial dislocations while the others splits into a pair of 30° and 60° partial dislocations, respectively. The atomic configurations of 30° partial and 90° partial dislocations are shown in Figs. 1a and 1b, respectively. In these figures, the reconstruction defects "solitons" are presented near the center of the figures. All the partials are separated by intrinsic stacking faults. The plastic flow occurs, primarily, through the motion of 30° and 90° glide partials lying on {111} planes. These partials, which have line directions along <110> are believed to be reconstructed into a structure with no dangling bonds. In view of this, we have performed the electronic structure calculations of glide 30° and 90° partial dislocations, taking into account the possibility of core reconstructions.

The kinks are modelled by breaking and forming bonds in such a way that the stacking fault is advanced to the next Peierls valley [18]. Figures 2 and 3 show the kink pair structure along the 90° and 30° partial, respectively. It is noted that there are two types of kinks along the 30° partial. Two five-membered rings are placed through the formation of the double kink by a four- and six-membered ring at A and by a five- and six-membered ring at B. The kinks along the 90° partial have identical structures and can be described as a transfer of two six-membered rings to a five- and a seven-membered ring. The kinks are fully coordinated and have the same local geometry for trailing and leading partials.

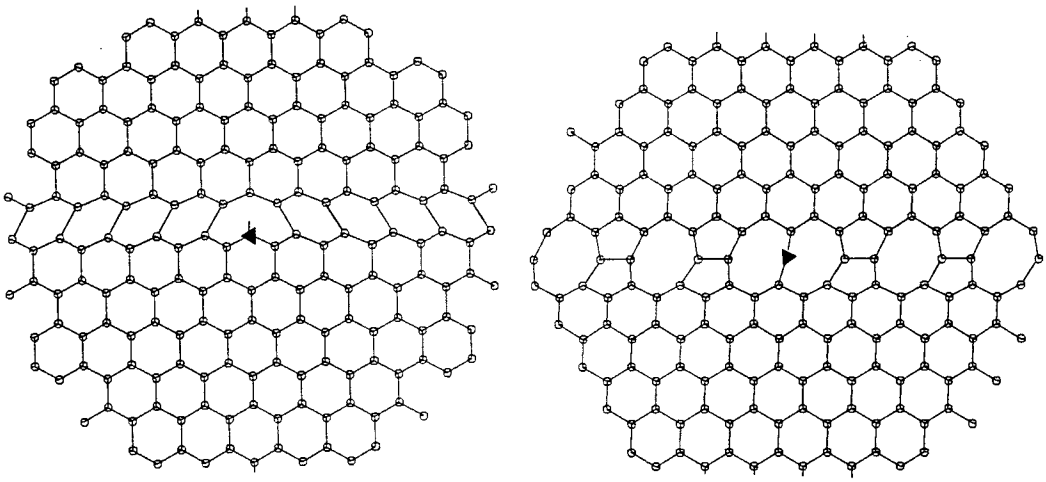

Fig.1 Atomic configurations of reconstructed 90° partial (a) and 30° partial (b) dislocations in diamond cubic lattice. The reconstruction defects "solitons" are also presented.

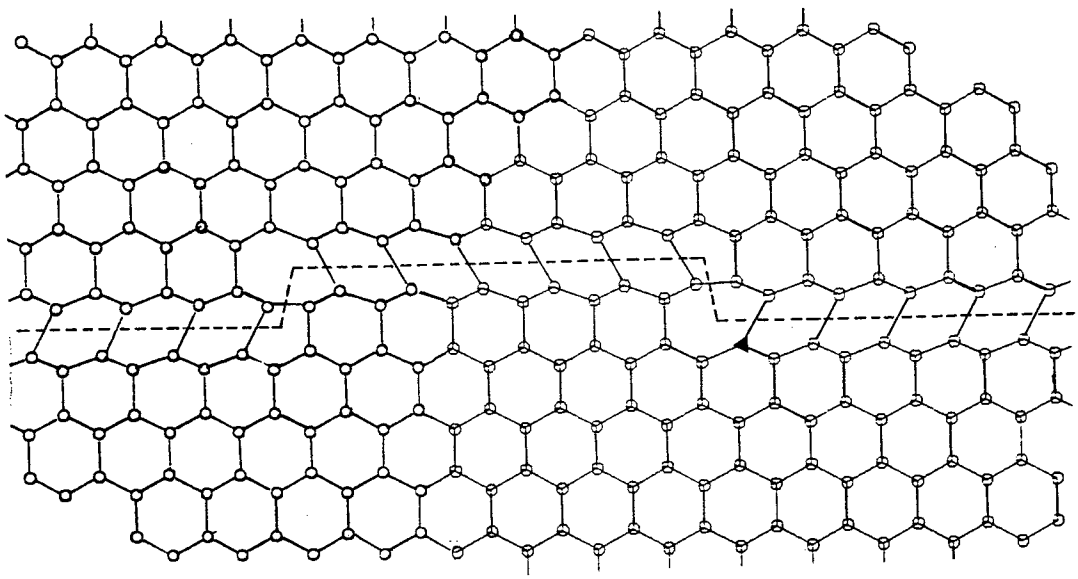

Fig.2 Atomic configurations of a double kink along the 90° partial dislocation in Si crystal.

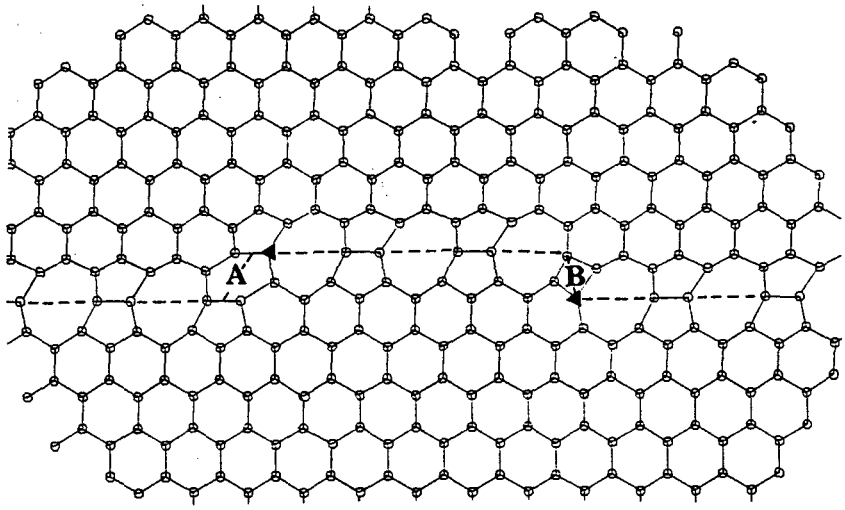

Fig.3 Atomic configurations of a double kink along the 30° partial. Note that the two kinks, marked by A and B, have inequivalent structures.

3a. Elemental Process of Dislocation Motion

Before discussing the electronic states of the dislocations, we briefly summarize the recent theories of enhanced dislocation motion in the semiconductors. The dislocation motion in covalent semiconductors has been discussed in detail by Hirth and Lothe [19] on the basis of the abrupt kink model and the kink diffusion theory of Peierls mechanism. The dislocation velocity is generally written in two different forms according to whether the kink-kink collision occurs or not

$$v = \begin{cases} 2d\sqrt{Jv_k} & (X<<L) \quad , \qquad (5\text{-a}) \\ dJL & (X>>L) \quad . \qquad (5\text{-b}) \end{cases}$$

Here J is the frequency of kink-pair formation per unit length of the dislocation, v_k is the lateral velocity of a kink along the Peierls valley, d is the interval of Peierls valleys, X is the mean free path of migration of a kink, and L is the segment length of a dislocation. The condition X<<L and X>>L, respectively, correspond to the dislocation motion with and without kink-kink collisions. Maeda and Takeuchi [5] have derived J directly from a set of rate equations which represent the equilibrium jump frequency of kinks at each kink site (0,1,2,... in Fig.4). The result of J is written as

$$J = \nu_S(bd\tau/kT)\exp\left[-\frac{1}{kT}\right]\left\{\sum_{i=0}^{p-1}\left(\Delta E_{i+}-\Delta E_{(i+1)-}\right)+E_{dif}\right\} \qquad (6)$$

where ν_s is the trial jump frequency of straight-dislocation sites, b is the Burgers vector, τ is the shear stress component in the direction of b, and E_{dif} is the effective activation energy barrier to diffusive kink migration. In the summation of the above eq.(6), p is the site number at which the energy of a kink pair assumes the maximum value, ΔE_{i+} and $\Delta E_{(i+1)-}$ denote the potential barriers to the processes of site i →site (i+1) and site i←site (i+1), respectively. On the other hand, the lateral kink velocity v_k is obtained by means of the Einstein relation in diffusive phenomenon.and given in a form of the Ahrenius type, with activation energy of E_{dif}.

$$v_k = \nu_k(bd\tau/kT)a^2 \exp[-E_{dif}/kT] , \qquad (7)$$

where ν_k is the trial jump frequency of kinks. One can then discuss the elementary process of the dislocation motion by estimating J and v_k, i.e., the summation term and E_{dif} in eq.(6) taking into account the experimental conditions.

Maeda and Takeuchi [5] have also derived expressions of the velocity of enhanced dislocation motion under crystal excitation. Since the electronic states of straight-dislocation sites are generally different from those of kink sites, recombination enhanced dislocation motion can be classified in the following three cases: (i) Recombination enhancement occurs at both straight-dislocation sites and kink sites, (ii) Recombination enhancement occurs only at straight-dislocation sites, and (iii) Recombination enhancement occurs only at the kink sites. In Table 2, we summarize the features of the enhanced dislocation motion of the above three cases. Then using the theoretical results

Table 2. Activation energies of enhanced dislocation motion (from Ref.5).

segment length	site of recombination	pre-exponential factor	reduction of activation energy
X<<L	SD + K	$\propto$ I	$(1/2)(\Delta E_S+\Delta E_k)$
	SD	$\propto \sqrt{I}$	$(1/2)\Delta E_S$
	K	$\propto \sqrt{I}$	$(1/2)\Delta E_k$
X>>L	SD + K	$\propto$ I	ΔE_S
	SD	$\propto$ I	ΔE_S
	K	no effect	no effect

SD: straight-dislocation site, K: kink site, I: excitation intensity.

presented in Table 2, and the facts that (i) X>>L is realized under usual experimental conditions and (ii) the pre-exponential factor is propotional to the excitation intensity I, one can show that the reduction in activation energy is simply equal to ΔE_s [20]. Here, ΔE_s denotes the decrease of the potential barrier under the crystal excitation for the process of site 0→ site 1. It is noted that ΔE_s takes larger value of ΔE_{se} and ΔE_{sh} (energy release of electron and hole captures, see Fig.5):

$$\Delta E_s = \max(\Delta E_{se}, \Delta E_{sh}) \qquad (8)$$

On the other hand, the potential barrier for the kink migration might be reduced by ΔE_k for the processes of site i ↔ site(i+1) (i=1,2,3,...) and site 0 ←site 1. However, it is noted that even if the enhancement of kink migration occurs, it does not contribute to the dislocation mobility enhancement because of the cancellation between the forward and backward kink migration.

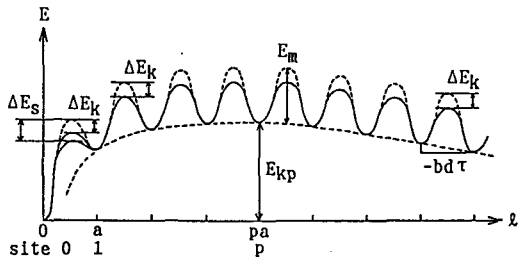

Fig.4 Potential barriers for dislocation motion in semi-conductors. Dashed line is estimated by using continuum elasticity theory.

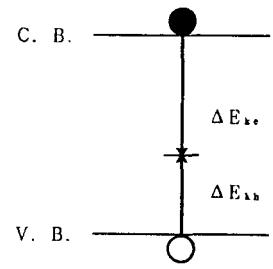

Fig.5 Non-radiative recombination at the straight dislocation sites.

3b. Electronic States and Dislocation Motion

In Figs.6 and 7, we present the local DOS of the perfect Si and C (diamond cubic) crystals, respectively. One can see in these figures that the lower valence band is composed mainly of s- and p- components, while the higher conduction band of s-, p- and s* components. Although the calculated DOS by the recursion method does not vanish exactly in the gap, we have obtained reasonable width of the energy gap region (with negligible DOS value), 1.17 eV and 5.2 eV, for Si and C crystal, respectively. The relative contributions of s-, p-(p_x+p_y+p_z) and s*- subbands to the total DOS of C crystal are quite similar to those of Si crystal, but the prominent three peaked valence band structure is obtained only for the Si crystal (not for C).

In Fig.8, we present the calculated local electronic DOS on the atom (with geometrical dangling bond) in the core of 90° partial dislocation in Si, together with s*- (8a), s- (8b) and p- (8c) partial DOS. It can be seen in this figure that there is no

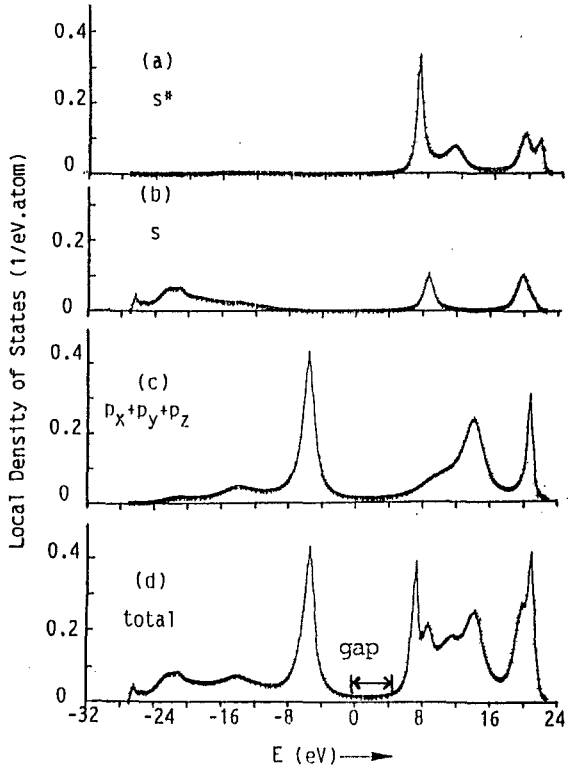

Fig.6 Electronic DOS of perfect C crystal, calculated by using sp^3s^* basis recursion method.

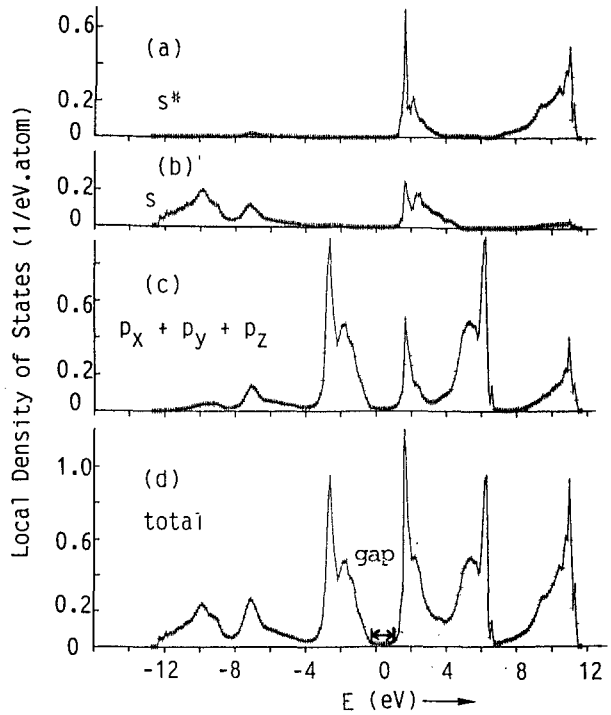

Fig.7 Electronic DOS of perfect Si crystal, calculated by using sp^3s^* basis recursion method.

prominent deep levels in the band gap region. Instead, we have obtained finite DOS in the gap region, in agreement with the previous theoretical calculations [21-22]. This may indicate that there can be electric currents along the dislocation line (so-called leakage current in the electronic device engineering). However, it must be noted that such electronic states in the gap region do not provide recombination centers which cause the enhanced dislocation mobility. We have also obtained the similar results for 90° partial dislocations in C crystal.

In Fig.9, we present the calculated local electronic DOS on the soliton-site atom (marked by Δ in Fig.1c) in the core of 90° partial dislocation in Si, together with s*-(9a), s-(9b) and p-(9c) partial DOS. One can see in Fig.9 that s- and p- (and s*) partial DOS are strongly deformed due to the variation of the atomic configuration of the dislocation core. In these calculations, it is the most important that the prominent deep levels of "solitons" (located near the center of the band gap) appear even for the reconstructed core with small atomic displacements of $\Delta<0.1d_0$ (d_0 being the nearest-neighbour distance of the perfect Si lattice).

The local DOS on the kink-site atom in the core of 90° partial dislocation in Si are shown in Fig.10. One can see in Fig.10 that finite DOS appear in the band gap region, but there are no δ-function like peaks in the gap. Although this kink-site atom has three nearest neighbours d_i ($i=1,2$, and 3) $> 1.25d_0$, it has a strongly compressed bond with $d_i \sim 0.92d_0$. Therefore, this atom has effectively no dangling bonds and does not produce any δ-function like gap states.

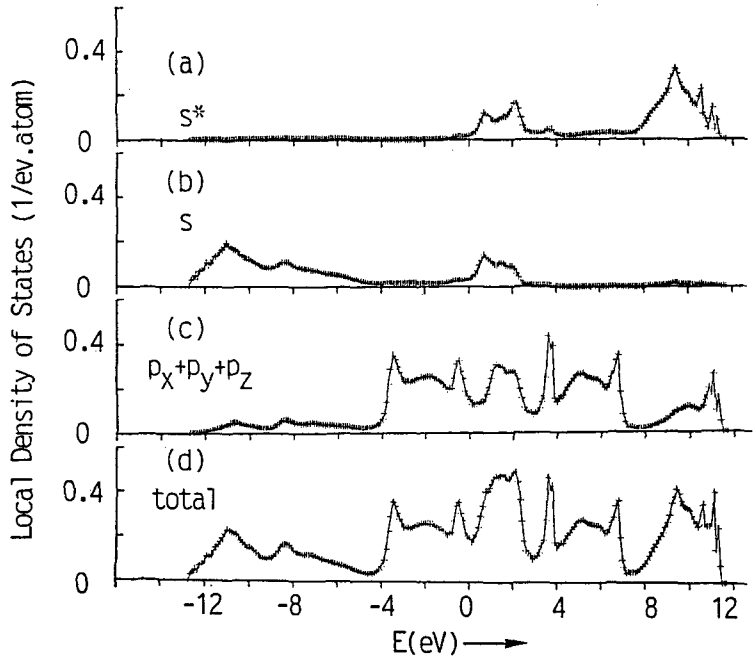

Fig.8 Local DOS on the atom in the core of the 90° partail dislocation in Si crystal (non-soliton site).

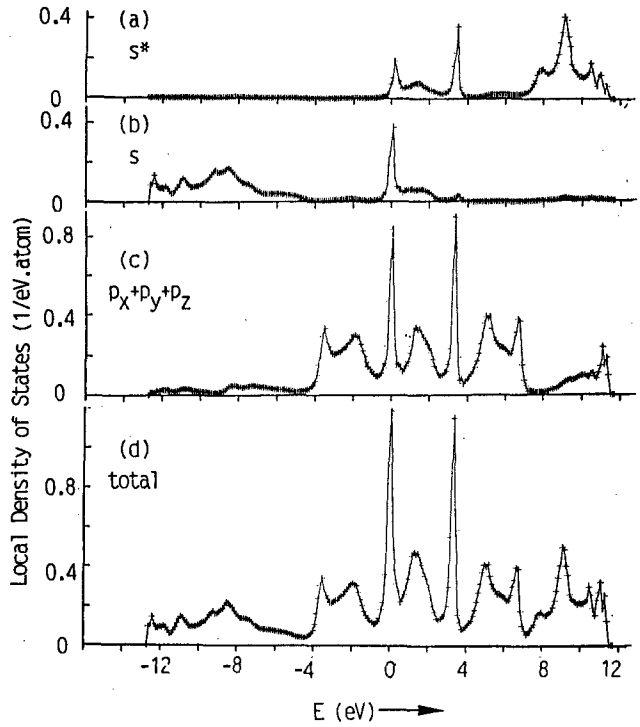

Fig.9 Local DOS on the atom in the core of 90° partial dislocation in Si crystal (soliton site).

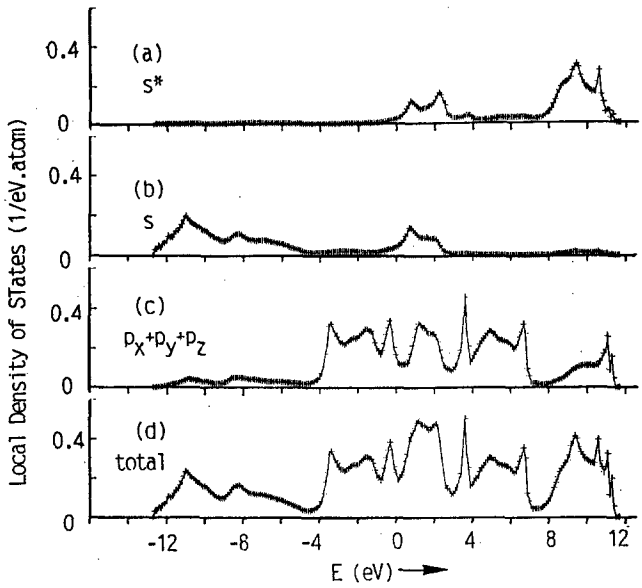

Fig.10 Local DOS on the kink-site atom in the core of 90° partial dislocation in Si crystal.

In Fig.11a, we present the local DOS on the soliton-site atom in the core of 30° partial dislocation in Si crystal. One can see in this figure that there appears a prominent deep level near the center of the gap. In Figs.11b and 11c, we also present the local DOS on the kink-site atoms A and B in the core of 30° partial dislocation in C crystal. We do not present here the DOS curves on kink-site atoms of 30° partial dislocation in Si crystal because they are quite similar to those of C crystal presented in Figs.11b and 11c. For the kink sites A and B, we do not have the deep levels in the gap. This is due to the fact that there are four nearest-neighbours on the kink-site atoms A and B (two compressed and two stretched bonds), and the electronic states are not changed strongly as in the atomic sites with geometrical dangling bonds.

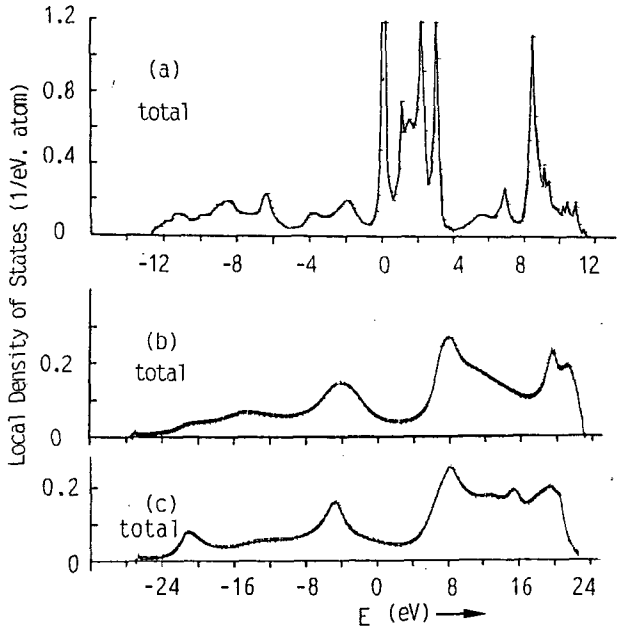

Fig.11 Local DOS on the kink-site atom in the core of 30° partial dislocation in Si: (b) and (c) are the local DOS on the kink-site atoms A and B in C crystal, respectively.

Summarizing the above mentioned electronic structure calculations of the dislocations, we can say that there are deep centers (associated with the reconstruction defects "solitons") along the straight dislocation line in much smaller density than the geometrical dangling bonds. We do not always have the deep levels associated with the kink-sites (point like singularities along the dislocation line) in the semiconductors C and Si. This is in consistent with the experimental results that the observed reduction in the activation energy (0.68-0.82eV for intrinsic Si) of the enhanced dislocation motion under irradiation of electron beam or laser light corresponds to the deep energy levels associated with the straight dislocation sites (rather than the kink sites) [5].

4. CONCLUSIONS

Using the LCAO recursion method of sp^3s^* basis orbital, we have investigated the atomic configurations and electronic states of dislocation in covalent semiconductors. Particular attention has been paid on the determination of gap states associated with the straight dislocation line as well as the point-like singularities like "soliton" or kink-site atoms. It is shown that point like singularities "solitons" in the dislocation core can produce prominent deep levels in the band gap, and they are expected to act as (non-radiative) recombination centers of the injected carriers. Although such possibility has already been pointed out by Jones et al. [8], the present theoretical findings are distinct from the previous ones, since the prominent deep centers can appear for the reconstructed dislocation core with small atomic displacements. Furthermore, we have found that the kink-site atom do not always produce the deep levels in the gap region because there are four nearest-neighbour atoms and cancellation of the electronic effects occurs from compressed and stretched bonds. In conclusion, the present theoretical calculations are consistent with the previous theoretical analysis [5] on the recombination enhanced dislocation motion and the experimental observation on the reconstruction of the dislocation core in the covalent semiconductors.

REFERENCES

1. J.R. Patel and A.R. Chaudhuri, Phys. Rev. 143, 601 (1966).
2. J.R. Patel, L.R. Testardi and P.E. Freeland, Phys. Rev. B13, 3548 (1976).
3. K. Maeda and S. Takeuchi, Appl. Phys. Lett., 42, 664 (1983).
4. K. Maeda, M. Sato, A. Kubo and S. Takeuchi, J. Appl. Phys., 54, 161 (1983)
5 N. Maeda and S. Takeuchi, Inst. Phys. Conf. Ser. No.104, Chapter 3, 303 (1989).
6. R. Haydock, V. Heine and M.J. Kelly, J. Phys. C5, 2845 (1972); C8, 2591 (1975).
7. K. Masuda-Jindo, Phys. Rev. B41, 8407 (1990).
8. M. Heggie and R. Jones, Phil. Mag., B48, 365, 379 (1983).
9. S. Takeuchi, private communication.
10. L. Verlet, Phys. Rev. 159, 98 (1967).
11. J.S. Luo and B. Legrand, Phys. Rev. B38, 1728 (1988).
12. S. Sawada, Vacuum, 41, 612 (1990).
13. M. Kohyama, J. Phys. 3, 2193 (1991).
14. L. Goodwin, A.J. Skinner and D.G. Pettifor, Europhys. Lett. 9, 701 (1989).
15. P. Vogl, H.P. Hjalmarson and J.D. Dow, J. Phys. Chem. Solids, 44, 365 (1983).
16. N. Beer and D.G. Pettifor, "Electronic Structure of Complex Systems", ed. by P. Phariscau and W.M. Temmerman, Plenum Press, New York, (1984), P.769.
17. H. Alexander and P. Haasen, Solid State Phys., 22, 27 (1968).
18. S. Marklund, Solid State Commun., 54, 555 (1985).
19. J.P. Hirth and J. Lothe, Theory of Dislocations (McGraw Hill, New York, 1968) P.531.
20. H. Sumi, Phys. Rev. B27, 2374 (1983).
21. H. Veth and H. Teichler, Phil. Mag. B49, 371 (1984).
22. Y. L. Wang and H. Teichler, phys. stat. sol., 154(b) 649 (1989).